ADVANCED FUNCTIONAL MATERIALS
www.afm-journal.de

Light-Up Probe for Targeted and Activatable Photodynamic Therapy with Real-Time In Situ Reporting of Sensitizer Activation and Therapeutic Responses

Youyong Yuan, Chong-Jing Zhang, Ryan T. K. Kwok, Shidang Xu, Ruoyu Zhang, Jien Wu, Ben Zhong Tang, and Bin Liu**

Integrated systems that offer traceable cancer therapy are highly desirable for personalized medicine. Herein, a probe is reported that is composed of a red-emissive photosensitizer (PS) with aggregation-induced emission characteristics and a built-in apoptosis sensor with activatable green emission for targeted cancer cell ablation and real-time monitoring of PS activation and therapeutic response. The probe is nonemissive in aqueous media and can be selectively uptaken by $\alpha_v\beta_3$ integrin overexpressed cancer cells. Cleavage of the probe by intracellular glutathione leads to release of the apoptosis sensor and red fluorescence turn-on to report the PS activation. Upon light irradiation, the PS can generate reactive oxygen species to induce cell apoptosis and activate caspase-3/-7, which will cleave the apoptosis sensor to yield intense green fluorescence. Both the red and green emission can be obtained through a single wavelength excitation, which makes the probe very convenient for therapeutic protocol development.

1. Introduction

Targeted delivery, accurate assessment of active therapeutic agents, and in situ reporting of their therapeutic effects are of high importance in cancer therapy.[1] The capability to visualize the whole process will undoubtedly provide more useful information to further optimize and advance the therapy. However, our capability is still limited in answering precisely when, where and how the therapeutic agents are delivered as well as what is their therapeutic effect. To realize targeted delivery, drug conjugates or drug encapsulated carriers with surface targeting moieties have been developed.[2] Fluorescent dyes and quantum dots have been further used to label these carriers or drugs to study their targeting effect and biodistribution.[3,4] Recently, fluorophore and drug conjugates with tumor-responsive linkers have been developed for real-time monitoring of activated drug concentration in cancer cells.[5–11] In addition, by incorporation of apoptosis sensors or apoptotic markers (e.g., ethidium) into prodrugs or nanoparticles, in situ monitoring of the drug therapeutic effect has also been realized.[12,13] Despite of the great efforts made toward smart probe design for traceable cancer therapy, most of the approaches can only monitor one of the processes. It remains challenge to develop a single molecular probe that is able to simultaneously detect, image, ablate cancer cells, and report the therapeutic response in situ.

Among the various therapeutic drugs under study, photosensitizer (PS) drugs have recently attracted increasing attention because photodynamic therapy (PDT) does not acquire drug resistance and it can be controlled with light irradiation.[14,15] PDT is based on the concept that PSs generate cytotoxic reactive oxygen species (ROS) upon light irradiation to induce cell death which is a powerful strategy for cancer treatment.[14,15] Over the years, although some fluorescent probes have been developed for ROS detection,[16–18] it remains challenge to monitor ROS generation in real-time and in situ in living systems due to the extremely short lifetime (<40 ns)

Dr. Y. Yuan, Dr. C.-J. Zhang, S. Xu, R. Zhang, Prof. B. Liu
Department of Chemical and Biomolecular Engineering
National University of Singapore
4 Engineering Drive 4, Singapore 117576, Singapore
E-mail: cheliub@nus.edu.sg
Dr. R. T. K. Kwok, Prof. B. Z. Tang
Department of Chemistry
Institute for Advanced Study
State Key Laboratory of Molecular Neuroscience
Institute of Molecular Functional Materials
Division of Biomedical Engineering
The Hong Kong University of Science and Technology
Clear Water Bay, Kowloon, Hong Kong, China
E-mail: tangbenz@ust.hk

DOI: 10.1002/adfm.201502728

Dr. J. Wu
Department of Chemistry
3 Science Drive 3
National University of Singapore
Singapore 117543, Singapore
Prof. B. Z. Tang
SCUT–HKUST Joint Research Laboratory
Guangdong Innovative Research Team
State Key Laboratory of Luminescent Materials and Devices
South China University of Technology
Guangzhou 510640, China
Prof. B. Liu
Institute of Materials Research and Engineering
Agency for Science
Technology and Research (A*STAR)
3 Research Link, Singapore 117602, Singapore

and small radius of action (<20 nm) of ROS.[19] There is thus very limited strategies reported to provide in situ monitoring of the therapeutic effect of PDT.[20] In addition, the currently available PSs frequently cause unwanted normal cell death due to their intrinsic phototoxicity and lack of selectivity for cancer cells.[14] As a consequence, targeted and/or activatable PSs with high therapeutic efficiency to cancer cells but minimized side effects to normal cells are subsequently reported.[21–25] However, the integration of all the desired properties into a single molecular probe that is able to simultaneously target and image cancer cells, report the PS activation and predict the therapeutic response in situ remains a grand challenge.

To visualize multiple processes in cancer therapy, fluorophores exhibiting different fluorescence upon a single wavelength excitation are highly desirable as they can minimize the complexity of fluorescence imaging by offering simultaneous detection. The design principle of traditional fluorescent probes often requires a pair of fluorescent dyes (energy donor/acceptor or donor/quencher) or relies on photoinduced electron transfer (PET) mechanism to visualize a single biological event, which makes it difficult to develop one molecular probe for monitoring multiple processes.[26] This calls for the development of multifunctional materials, where a single molecule can be used to report an event or even also born with therapeutic functions. It is fortunate that the recent development of fluorogens with aggregation-induced emission characteristics (AIEgens) offers such an opportunity.[11,27–33] AIEgens show almost no fluorescence as molecular species, but bright fluorescence in aggregate state due to restriction of intramolecular motions and prohibition of energy dissipation via nonradiative channels.[34] Taking advantages of the unique properties of AIEgens, we have developed light-up probes without incorporation of any quencher moiety or energy transfer pairs.[27,28] More recently, we and other groups also reported functional AIEgens with tunable emissions, and demonstrated that they could be used as potential chemo-drugs or PSs for chemotherapy and PDT.[35–37]

In this contribution, we developed an AIEgen based probe, namely TPETP-SS-DEVD-TPS-cRGD (**Figure 1**), for targeted imaging, activatable and traceable cancer cell PDT with additional capacities of real-time self-reporting of PS activation and therapeutic responses upon a single wavelength excitation. Tetraphenylethenethiophene (TPETP) is a red-emissive AIEgen with photosensitization property, while tetraphenylsilole (TPS) is an iconic green emissive AIEgen[27] and both could be excited with a 405 nm laser to yield distinct emission peaks. As ROS could cause cancer cell death through apoptosis pathway within a short period of time,[38–40] and caspases-3/7 are key mediators of cell apoptosis,[41] a caspase-3/-7 responsive peptide substrate DEVD based apoptosis sensor is incorporated into the probe. In addition, c-RGD and –S–S– are used as the targeting ligand and linker to realize dual-targeted activatable PDT. Upon c-RGD mediated cellular uptake, the –S–S– bond can be cleaved by glutathione (GSH) to yield red fluorescence turn-on of the PS and release the apoptosis sensor. Consequently, the activated caspases cleave the DEVD substrate on the probe and release hydrophobic TPS residue with intense green fluorescence to report the therapeutic effect. As compared to the recent report of a lysotracker and PS coencapsulated nanoparticles for monitoring of the therapeutic responses of PDT *via* a fluorescence-off signal,[20] our distinct fluorescence turn-on signal is more desirable in complicated biological systems.

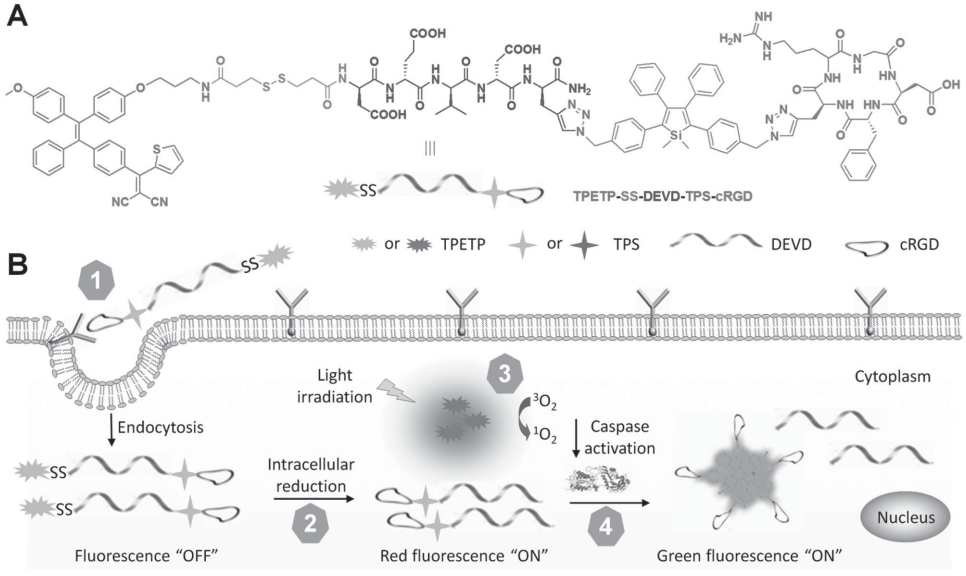

Figure 1. Schematic illustration of the dual-targeted probe for real-time and in situ monitoring of PS activation and the therapeutic responses. A) The chemical structure of the probe TPETP-SS-DEVD-TPS-cRGD; B) The probe functions in four steps: (1) receptor mediated endocytosis of the probe; (2) cleavage of the disulfide bond through intracellular reduction by glutathione to release the nonemissive apoptosis sensor and the PS with red fluorescence; (3) upon light irradiation, ROS generation to induce cell apoptosis and activate caspase enzymes; (4) cleavage of the DEVD substrate by the activated caspases on the apoptosis sensor to result in green fluorescence turn-on. The red fluorescence of the TPETP residue can be used for image-guided photodynamic therapy while the green fluorescence of TPS can be used for the therapeutic response imaging. The structures of TPETP and TPS residues are shown in the Scheme S1, Supporting Information.

2. Results and Discussion

2.1. Design Principle of the AIEgen PS and the Probe

The design principle of the AIEgen PS is based on the following two considerations: AIE characteristics with efficient ROS generation, and the same excitation but distinct emission wavelengths from those of TPS. Build upon tetraphenylethylene (TPE), one of the most commonly used AIEgens with UV absorption and weak ROS generation,[42] introducing dicyanovinyl group as an electron acceptor (A) and methoxy group as an electron donor (D) into a TPE core forms a D–π–A structure, which is expected to yield a new AIEgen with red shifted absorption/emission maxima. In addition, the D–π–A structure can lead to small $\Delta E_{S1\text{-}T1}$ (energy gap between the lowest singlet excited state (S_1) and the lowest triplet excited state (T_1) states), which is favorable for intersystem crossing (ISC) to yield efficient ROS generation.[43] The molecular structures, HOMO and LUMO distribution and $\Delta E_{S1\text{-}T1}$ values of TPE (1.22 eV), TPS (1.27 eV) and TPETP (0.29 eV) are summarized in **Figure 2**. TPETP exhibits a much smaller $\Delta E_{S1\text{-}T1}$ compared with TPE, suggesting a potentially high ISC rate and thus possibly efficient ROS generation upon light irradiation.[44] The probe design principle is illustrated in Figure 1. The probe is composed of five components: (1) a red emissive TPETP to serve as a visualizing agent and a PS; (2) a disulfide linker, which can be cleaved by GSH overexpressed in cancer cells; (3) a highly hydrophilic DEVD substrate that can be specifically cleaved by caspase-3/-7; (4) a green emissive TPS molecule to serve as the signal reporter for the apoptosis sensor; and (5) a hydrophilic cyclic arginine–glycine–aspartic acid (cRGD) peptide for targeting cancer cells with overexpressed $\alpha_v\beta_3$ integrin. The probe is water-soluble and shows very weak fluorescence in aqueous media. Once the probe is selectively taken up by $\alpha_v\beta_3$ integrin overexpressed cancer cells through receptor mediated endocytosis, the disulfide bond will be cleaved by intracellular GSH, which will release the apoptosis sensor and turn on the red fluorescence of the TPETP residue (Scheme S1, Supporting Information) as an indication of PS activation. Upon light illumination, the PS will generate ROS, which induces the cell apoptosis and activates caspase-3/-7. The caspases will then cleave the DEVD substrate to result in green fluorescence turn-on of the TPS residue (Scheme S1, Supporting Information), which is able to real-time report the therapeutic efficiency of PDT. Considering that the overall process can be monitored with a single wavelength excitation, the probe thus offers a unique opportunity for targeted and activated cancer therapy with real-time reporting of PS activation and therapeutic responses.

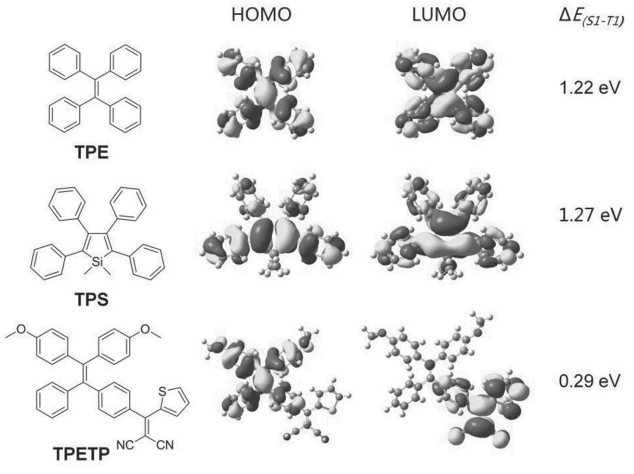

Figure 2. Chemical structures and HOMO–LUMO distribution of tetraphenylethene (TPE), TPS, and TPETP, optimized structures of the HOMO and LUMO at S_1 were calculated by time-dependent DFT (Gaussian 09/B3LYP/6–31G(d)).

2.2. Synthesis of TPETP-NH_2 and Identification of the Isomer

The two isomers of TPETP-NH_2 (*cis*-TPETP-NH_2 and *trans*-TPETP-NH_2) were synthesized as depicted in **Figure 3**. Briefly, compound **1** was treated with *n*-butyllithium, trimethyl borate, and diluted HCl to yield compound **2** with boronic acid functionality, which underwent palladium-catalyzed coupling with 2-thiophenecarbonyl chloride to yield compound **3**. Compound **3** was further treated with $TiCl_4$ and malanonitirile to generate compound **4** with a dicyanovinyl group, which was subsequently treated with BBr_3 to yield compound **5** with one free hydroxyl group. The reaction between compound **5** and 3-(boc-amino) propyl bromide furnished compound **6**, which was reacted with trifluoroacetic acid (TFA) to deprotect the Boc group and yield the mixture of *cis* and *trans* isomers of TPETP-NH_2. The compounds **1–6** were characterized by NMR and mass spectroscopies (Figures S1–S4, Supporting Information). The two isomers of TPETP-NH_2 were separated by preparative high-performance liquid chromatography (HPLC) as red powders after freeze drying (Figures S5 and S6, Supporting Information). After measuring ^{1}H COSY and NOESY NMR for the major isomer, all the peaks with different chemical shifts were assigned (Figures S7–S9, Supporting Information). As shown in the NOESY spectrum (**Figure 4**), the H-3&5 have strong correlations with the H-21&25, which suggest that the rings A and C are on the same side. Since there was no significant difference in fluorescence and ROS generation ability between the two isomers (Figure S10A,B, Supporting Information), the major isomer of *cis*-TPETP-NH_2 was used for the subsequent modification.

2.3. Synthesis of the Probe

Azide-functionalized TPS (TPS-$2N_3$) was prepared according to our previous report.[45] The double "click" reactions between TPS-$2N_3$ and alkyne-functionalized cRGD as well as alkyne-functionalized DEVD were catalyzed by $CuSO_4$/sodium ascorbate in DMSO/water mixture (v/v = 10/1), which afforded the apoptosis sensor DEVD-TPS-cRGD in 42% yield after HPLC purification. Furthermore, asymmetric functionalization of dithiobis(succinimidyl propionate) (DSP) with TPETP-NH_2 and the DEVD-TPS-cRGD afforded the target probe, TPETP-SS-DEVD-TPS-cRGD in 32% yield as red powders. The HPLC and mass spectra confirmed the right structures of the probe and intermediates with high purity (Figures S11–S14, Supporting Information).

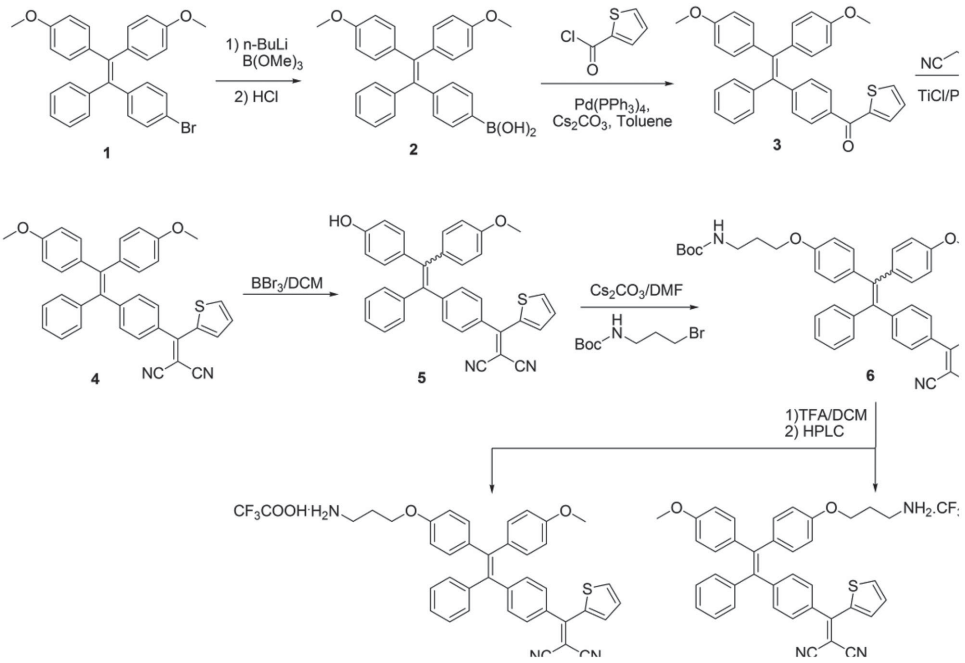

Figure 3. Synthesis of *cis*-TPETP-NH_2 and *trans*-TPETP-NH_2.

2.4. Optical Properties of the Probe and its Activation by GSH

The absorption and emission spectra of *cis*-TPETP-NH_2 in DMSO/water mixtures (v/v = 1/199) are shown in **Figure 5**A. The UV–vis absorption of *cis*-TPETP-NH_2 covers the range of 400–500 nm with a shoulder peak at 430 nm. The PL spectrum is ranged from 550 to 850 nm with an emission maximum at 650 nm and the quantum yield (Φ) is determined to be 0.13 using 4-(dicyanomethylene)-2-methyl-6-(4-dimethylaminostyryl)-4*H*-pyran (DCM) as the reference (Φ = 0.43 in water). To study whether *cis*-TPETP-NH_2 retains the AIE property, its PL spectra in DMSO/water mixtures were monitored at the same compound concentration but with different water fractions (f_w). As shown in Figure 5B, *cis*-TPETP-NH_2 is almost nonemissive in its benign solvent DMSO. This is attributed to the free motions of *cis*-TPETP-NH_2 in molecularly dissolved state. The fluorescence of *cis*-TPETP-NH_2 increases quickly when the f_w is higher than 50 vol%. At f_w = 99 vol%, the fluorescence intensity of *cis*-TPETP-NH_2 is 120-fold higher than its intrinsic fluorescence in pure DMSO. The PL results demonstrate that *cis*-TPETP-NH_2 is AIE-active.

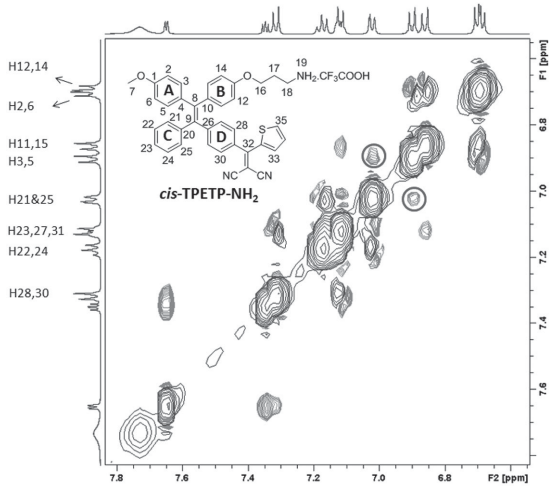

Figure 4. ^1H–^1H NMR NOESY spectrum of compound *cis*-TPETP-NH_2. Spots in red circles indicate strong correlation between H3&5 and H21&25.

The PL spectra of *cis*-TPETP-NH_2 and the probe in DMSO/PBS mixtures (v/v = 1/199) are shown in Figure 5C. *cis*-TPETP-NH_2 shows intense red fluorescence. However, the probe TPETP-SS-DEVD-TPS-cRGD is almost nonemissive because of its good water-solubility due to the attached hydrophilic DEVD and cRGD peptides. The significant difference in the PL spectra of the probe and *cis*-TPETP-NH_2 inspired us to develop a cancer cell specific light-up probe based on cleavage of the disulfide bond by intracellular thiols. The fluorescence response of the probe toward GSH was studied first. As shown in Figure 5D, the red fluorescence of TPETP residue is increased steadily over 2 h upon addition of GSH to the probe solution. The fluorescence intensity reaches a plateau after 90 min incubation, which is 14-fold higher than the original intensity of the probe. The gradual enhancement of red fluorescence is ascribed to the increased amount of TPETP residue formed by cleavage of disulfide bond of the probe. Furthermore, the formation of TPETP aggregates was confirmed by laser light scattering (LLS) measurements. No LLS signals could be detected from the probe initially, while aggregates with an average diameter of 148 ± 12 nm were detected after GSH treatment (Figure S15A, Supporting Information). Subsequently, the probe at different concentrations was incubated with GSH for 90 min and the corresponding fluorescence changes were recorded. As shown

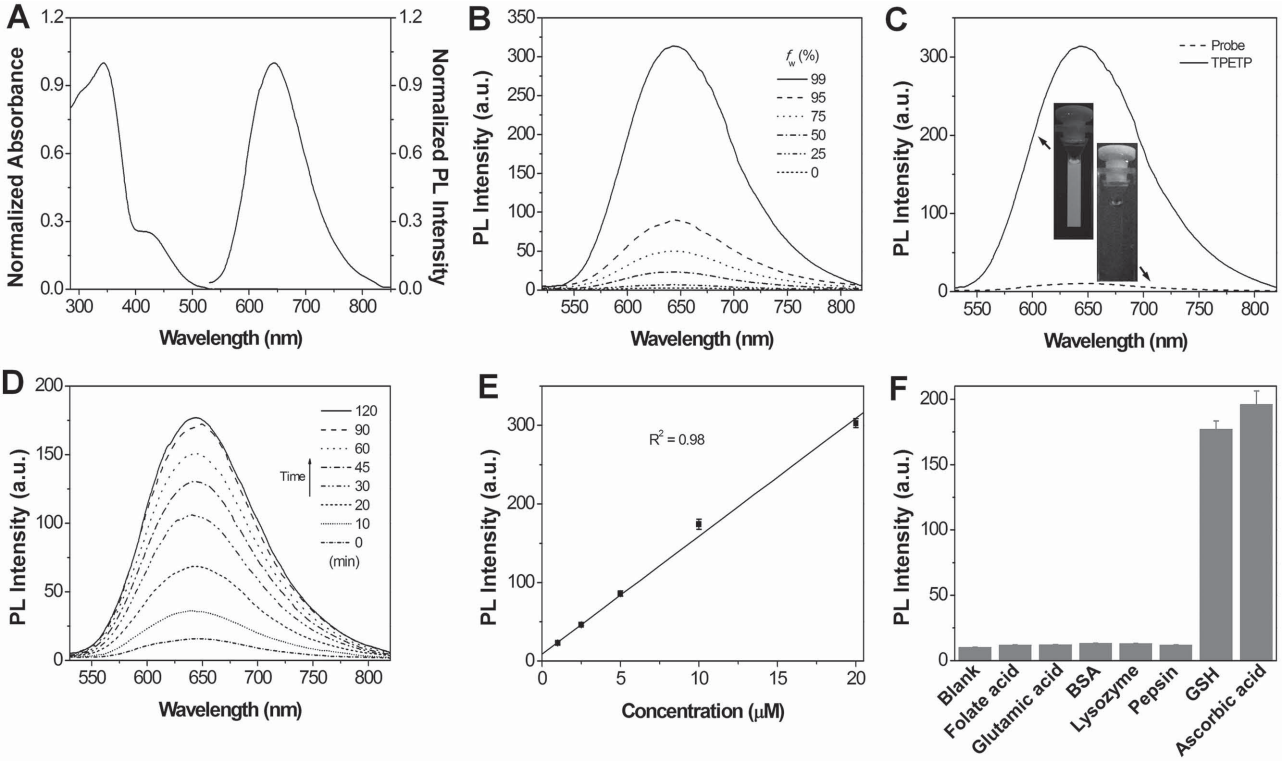

Figure 5. Optical properties of the probe and its responses to GSH and other analytes. A) Normalized absorption and emission spectra of *cis*-TPETP-NH_2 in DMSO/water mixtures (v/v = 1/199); B) Photoluminescence (PL) spectra of *cis*-TPETP-NH_2 in DMSO/water mixtures at different water fractions (f_w); C) PL spectra of *cis*-TPETP-NH_2 and the probe in DMSO/PBS mixtures (v/v = 1/199); D) Time-dependent PL spectra of the probe 10×10^{-6} M incubated with GSH (0.1×10^{-3} M); E) Plot of PL intensity at 650 nm for the probe at different concentrations upon incubation with GSH (0.1×10^{-3} M) in DMSO/PBS mixtures (v/v = 1/199) for 75 min; F) Change of PL intensity of the probe (10×10^{-6} M) upon incubation with glutamic acid, folate acid, lysozyme, bovine serum albumin (BSA), pepsin, ascorbic acid or GSH in DMSO/PBS mixtures (v/v = 1/199). The excitation wavelength was 430 nm for (A-F).

in Figure 5E, the plot of the PL intensities at 650 nm shows a linear relationship with the probe concentrations (R^2 = 0.98), indicating that the red fluorescence intensity could be used to quantify the amount of activated PS. The selectivity of the probe was subsequently studied, and the PL results revealed that the red fluorescence is only turned-on in the presence of reducing agents such as GSH and ascorbic acid while other bioacids and proteins show negligible fluorescence changes (Figure 5F). These results further support that the increase of red fluorescence in Figure 5D is due to the cleavage of the disulfide bond by the reducing agents.

The ROS generation of PSs upon light irradiation is a critical step for efficient PDT. The ROS quantum yield (Φ) of *cis*-TPETP-NH_2 in DMSO/PBS (v/v = 1/199) was determined to be 0.68 using Rose Bengal (RB) as the standard photosensitizer (Φ_{RB} = 0.75 in water), which is much higher than the clinically used PSs such as Photofrin (Φ = 0.28) or Laserphyrin (Φ = 0.48).[46] The ROS generation from the TPETP residue was also evaluated by measuring the absorbance of the solution containing the GSH pretreated probe and a ROS indicator, 9,10-anthracenediyl-bis(methylene)dimalonic acid (ABDA), in DMSO/PBS mixtures (v/v = 1/199) under light irradiation. As depicted in Figure S10C, Supporting Information, the absorption peaks of ABDA at 358, 378, and 400 nm decrease gradually upon light irradiation, as a result of fast reaction between the ROS generated by the TPETP residue and the anthracene moiety in ABDA. After 12 min irradiation, the absorbance at 400 nm is decreased to 22% of its original value. When vitamin C (a well-known ROS scavenger) is added, only 6% of the original ABDA absorbance is decreased under the same treatment, further confirming that ROS is generated by the TPETP residue upon light irradiation.

2.5. Caspase-3/-7 Activation of the Released Apoptosis Sensor

The absorption and emission spectra of TPS-$2N_3$ in DMSO/PBS (v/v = 1/199) buffer are shown in **Figure 6**A. TPS-$2N_3$ has absorption and emission maxima at 365 and 480 nm, respectively. The quantum yield (Φ) of TPS-$2N_3$ in DMSO/PBS (v/v = 1/199) is determined to be 0.28 using quinoline sulfate as the reference (Φ = 0.54 in 0.5 M H_2SO_4). Its PL spectra in DMSO/water mixtures with different f_w are shown in Figure 6B, which reveal that the fluorescence intensifies with the increased f_w value. The apoptosis sensor DEVD-TPS-cRGD shows much weaker fluorescence as compared to the same concentration of TPS-$2N_3$ in DMSO/PBS (v/v = 1/199) (Figure 6C). It should be noted that although the GSH-pretreated probe shows intense red fluorescence (Figure 5D, excitation at 430 nm), excitation of the same solution at 365 nm does not lead to obvious

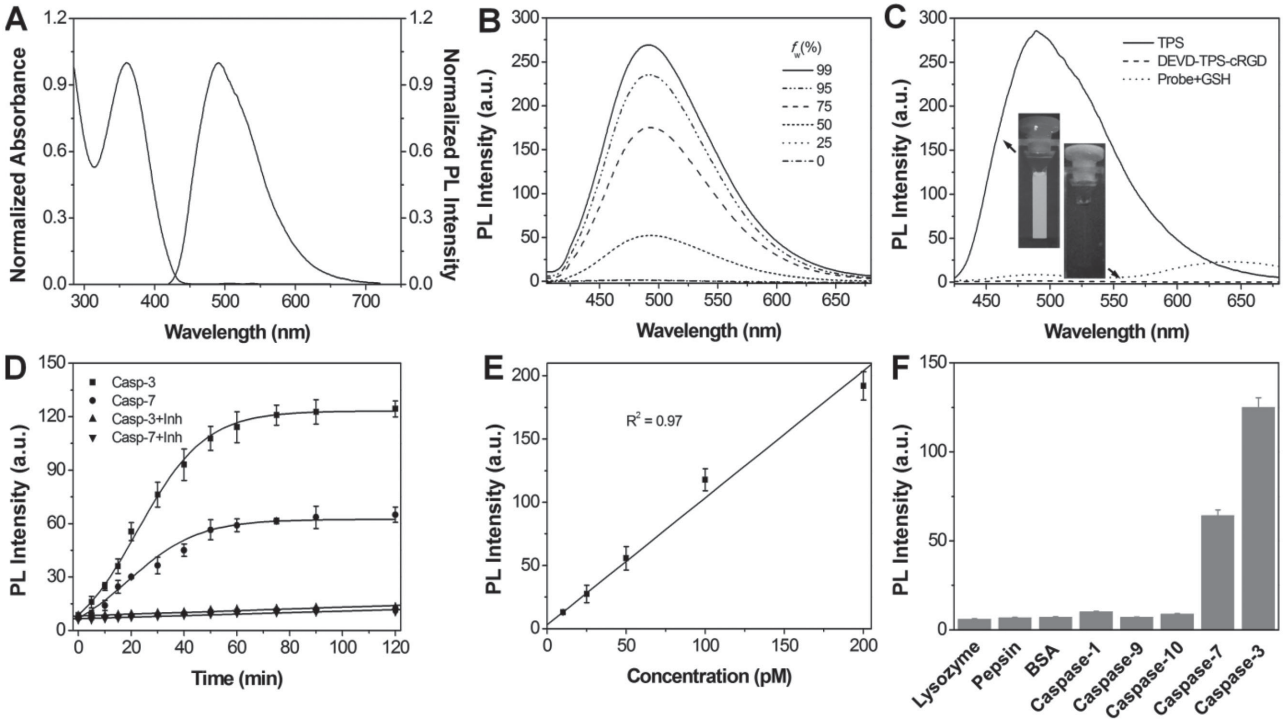

Figure 6. A) Normalized absorption and emission spectra of TPS-2N$_3$ in DMSO/water mixture (v/v = 1/199). B) PL spectra of TPS-2N$_3$ in DMSO/water mixtures with different water fractions (f_w). C) PL spectra of TPS-2N$_3$, apoptosis sensor DEVD-TPS-cRGD and the probe TPETP-SS-DEVD-TPS-cRGD in DMSO/PBS mixtures (v/v = 1/199). D) Time-dependent fluorescence spectra of GSH pretreated probe upon incubating with caspase-3 or caspase-7 with or without the addition of caspase-3/-7 inhibitor. E) PL intensities at 480 nm of GSH pretreated probe (10×10^{-6} M) upon incubation with various concentrations of caspase-3 for 60 min. F) PL intensities at 480 nm of GSH pretreated probe (10×10^{-6} M) toward different proteins or caspases. The excitation wavelength was 365 nm for (A-F).

green fluorescence (the broad emission above 600 nm is attributed to the TPETP residue), indicating that the release of the apoptosis sensor alone will not yield TPS fluorescence. However, a quick green fluorescence increase is observed when the GSH-pretreated probe (10×10^{-6} M) is further treated with caspase-3/-7 due to the release and aggregation of the hydrophobic TPS residue (Figure 6D), confirmed by LLS results (Figure S15B, Supporting Information). The TPS residue fluorescence reaches plateau after 60 min treatment of caspase-3 (100×10^{-12} M), which is 18-fold higher than the intrinsic fluorescence of the GSH-pretreated probe TPETP-SS-DEVD-TPS-cRGD (Figure 6D) upon excitation at 365 nm. In addition, the green fluorescence enhancement is prohibited in the presence of a highly specific caspase-3/-7 inhibitor 5-[(*S*)-(+)-2-(methoxymethyl)pyrrolidino]sulfonylisatin.[47] It is important to note that the fluorescence of GSH-pretreated probe at 480 nm intensifies upon incubation with increased concentrations of caspase-3 (Figure 6E). The plot of the PL intensities at 480 nm against caspase-3 concentrations gives a linear fit (R^2 = 0.97), suggesting that it is possible to semiquantify the concentration of caspase-3 through PL intensity changes. The detection limit of caspase-3 is 2.3×10^{-12} M estimated by three times standard deviation (3σ) method.

The selectivity of the apoptosis sensor DEVD-TPS-cRGD was evaluated by incubating the GSH-pretreated probe with pepsin, lysozyme, bovine serum albumin (BSA), and other caspases. As shown in Figure 6F, only caspase-3/-7 treated groups trigger fluorescence of the apoptosis sensor, indicating that the DEVD substrate is specifically cleaved by caspase-3/-7 when the cells undergo apoptosis. Since there are many kinds of enzymes in the cells, we also incubated the probe with cellular lysates of untreated and apoptotic (induced with 2×10^{-6} M staurosporine, STS) MDA-MB-231 cancer cells.[48] The fluorescence intensities at 480 and 650 nm were monitored after different periods of incubation. As shown in Figure S16, Supporting Information, the fluorescence intensities at 650 nm increase quickly in both the untreated and apoptotic cells confirming that the intracellular GSH can cleave the disulfide bond. On the other hand, the fluorescence enhancement at 480 nm is only observed when the probe is incubated with the apoptotic cell lysate.

2.6. Monitoring of Intracellular PS Release

To demonstrate the light-up imaging of specific $\alpha_v\beta_3$ integrin overexpressed cancer cells, the probe was incubated with $\alpha_v\beta_3$ integrin overexpressed MDA-MB-231 breast cancer cells and low $\alpha_v\beta_3$ integrin expressed MCF-7 breast cancer cells as well as 293T normal cells.[49] As shown in **Figure 7**, the red fluorescence from TPETP residues in MDA-MB-231 cells intensifies gradually with the increase of incubation time. In addition, the red fluorescence in MDA-MB-231 is much stronger than those in MCF-7 and 293T cells under the identical conditions. It is important to note that free TPETP can also be uptaken by

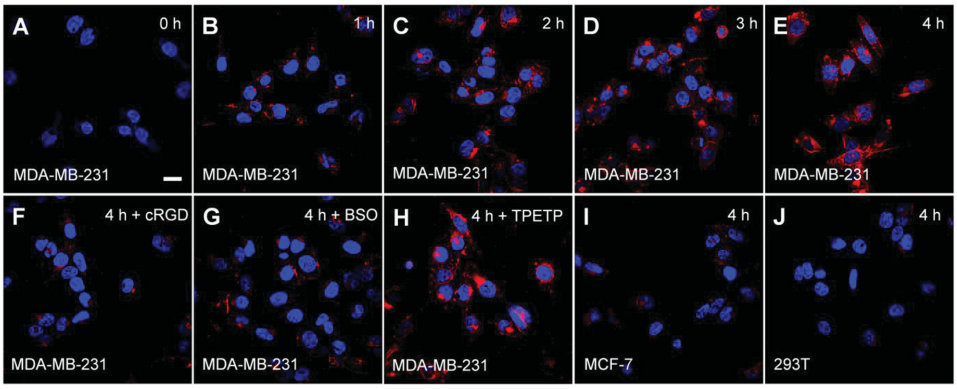

Figure 7. Confocal images of A–H) MDA-MB-231 cells, I) MCF-7 cells (I), J) 293T cells or MDA-MB-231 cells pretreated with cRGD (F) or BSO (G) after incubation with the probe (A–G, I, and J) or TPETP (H) for 0 h (A), 1 h (B), 2 h (C), 3 h (D), and 4 h (E–J). The blue fluorescence is from the cell nuclei stained with Hoechst (E_x: 405 nm; E_m: 430–470 nm); the red fluorescence is from the TPETP residue (E_x: 405 nm; E_m: > 560 nm). The scale bar is 20 μm.

MDA-MB-231 cells to yield strong red fluorescence (Figure 7H), and the fluorescence pattern is similar to that in Figure 7E. When MDA-MB-231 cells are pretreated with free cRGD prior to probe incubation, the red fluorescence in the cells is dramatically reduced. Similarly, the MDA-MB-231 cells show much weaker red fluorescence when the cells are pretreated with *g*-glutamylcysteine synthetase buthionine sulfoximine (BSO), which could inhibit the cells to produce GSH.[50] Moreover, flow cytometry analysis (Figure S17, Supporting Information) is used to further evaluate the probe specificity and the results are in well accordance with the confocal images shown in Figure 7. These results clearly demonstrate that the probe is specifically internalized by MDA-MB-231 cells through receptor mediated endocytosis and the red fluorescence is turned on by intracellular GSH, which can be used for PS activation monitoring and specific cancer cell imaging.

2.7. Imaging of Cell Apoptosis Induced by PDT

The intracellular ROS generation upon light irradiation in MDA-MB-231 cells was first evaluated by using 2′,7′-dichlorodihydrofluorescein diacetate (DCF-DA) as the indicator (Figure S18, Supporting Information). To explore the capability of using DEVD-TPS-cRGD as an apoptosis sensor, the MDA-MB-231 cells were pretreated with *cis*-TPETP-NH_2 (10×10^{-6} M) with light irradiation (1 min) or STS (1×10^{-6} M), then the cells were further incubated with DEVD-TPS-cRGD for 4 h. As shown in Figure S19, Supporting Information, strong green fluorescence of the TPS residue is observed in both STS and *cis*-TPETP-NH_2 treated MDA-MB-231 cells with light irradiation for the latter, indicating that apoptosis occurs in both cases. It should be noted that the DEVD-TPS-cRGD itself is of low cytotoxicity (Figure S20, Supporting Information), which does not induce cell apoptosis.

To further explore the possibility of the probe for PDT and in situ apoptosis imaging in $\alpha_v\beta_3$ integrin rich cancer cells, we incubated the probe with MDA-MB-231, MCF-7, and 293T cells for 4 h with light irradiation. The fluorescence changes of TPS in cells were monitored by confocal images. As shown in **Figure 8**, the green fluorescence of TPS residue in probe incubated MDA-MB-231 cells increases gradually with time when the cells are exposed to light irradiation. Together with that shown in Figure S16, Supporting Information, these results clearly indicate that the ROS generation of TPETP residue upon light irradiation can cause cell apoptosis and activate caspase-3/-7 to cleave the DEVD substrate. This is further confirmed by TPETP and cRGD-TPS-DEVD coincubated MDA-MB-231 cells, which show strong green fluorescence after light irradiation. On the contrary, only a weak fluorescent signal is detected in MCF-7 or 293T cells for more than 4 h of light irradiation. When MDA-MB-231 cells were pretreated with free cRGD or vitamin C prior to the probe incubation, the cells showed much weaker green fluorescence. This is because the free cRGD competes with the $\alpha_v\beta_3$ integrin receptor to the probe while vitamin C serves as a ROS scavenger to consume the ROS generated by the activated PS.

2.8. Imaging of Cell Apoptosis

To further confirm that the probe can image cell apoptosis, the probe incubated MDA-MB-231 cells after light irradiation were costained with anticaspase-3 primary antibody and a Texas Red-labeled secondary antibody. As shown in **Figure 9**A, the green fluorescence of the TPS residue and the red immunofluorescence signals from Texas Red are overlapped with high coefficient. When the cells are incubated with a caspase-3/7 inhibitor of 5-[(*S*)-(+)-2-(methoxymethyl)pyrrolidino]sulfonylisatin, followed by light irradiation, the green fluorescence of TPS residue is greatly reduced and only red fluorescence of Texas Red remains (Figure 9B). Overall, these results demonstrate that the ROS generation of TPETP residue can induce cell apoptosis and the activation of the caspase-3/7 has led to the green fluorescence turn-on of TPS residue, which can be used for self-reporting of cell apoptosis in situ.

2.9. Cell Death Prediction

The CytoTox-Fluor cytotoxicity assay was used to evaluate the correlation between cell viability and apoptosis after cell

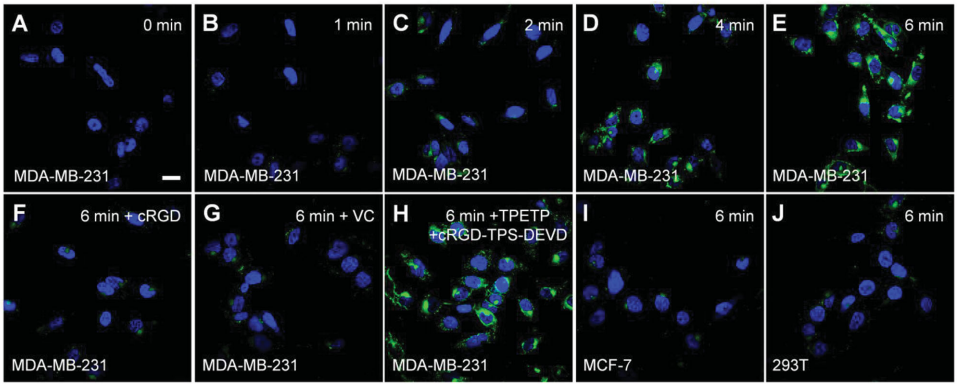

Figure 8. Confocal images of (A–H) MDA-MB-231 cells, I) MCF-7, J) 293T or MDA-MB-231 cells treated with cRGD (F) or VC (G) and upon incubation with the probe (A–G, I, and J) or TPETP and cRGD-TPS-DEVD (H) for 4 h with light irradiation of 0 min (A), 1 min (B), 2 min (C), 4 min (D), 6 min (E–J) at the power density of 0.10 W cm^{-2}. The blue fluorescence is from the nuclei of cells stained with Hoechst (E_x: 405 nm; E_m: 430–470 nm); the green fluorescence is from TPS residue (E_x: 405 nm; E_m: 505–525 nm).

incubation with the probe and light irradiation. The CytoTox-Fluor cytotoxicity assay can evaluate the cell viability using a fluorogenic peptide substrate (bis-alanyl-alanyl-phenylanlanyl-rhodamine 110; bis-AAF-R110). We studied the correlation between the R110 fluorescence intensity evaluated by the assay and the TPS residue fluorescence of the probe in MDA-MB-231 cells after light irradiation for different period of time. After the cells were incubated with the probe for 4 h and exposed to light irradiation for different time durations, the fluorescence intensities of R110 and the TPS residue were recorded by a microplate reader. As shown in **Figure 10**, the fluorescence intensity of R110 after different time of light irradiation correlates well with the apoptosis induced TPS residue fluorescence change, suggesting that the probe is capable of predicting the PDT-induced cell viability by measuring the TPS residue fluorescence intensity noninvasively. Therefore, the probe can be used to report its therapeutic response in situ.

3. Conclusions

We developed a multifunctional probe based on two AIEgens with distinguishable emissions for targeted cancer cell ablation and simultaneous real-time reporting of PS activation and therapeutic responses upon a single wavelength excitation. The probe itself is almost nonemissive in aqueous media due to the attachment of hydrophilic peptides, and the molecularly dissolved state facilitates free rotation of the phenyl rings contained in both AIEgens. Upon cRGD-mediated cellular uptake, the red fluorescence of TPETP residue is turned on as a result of the cleavage of the disulfide group by intracellular GSH, which has been used for cellular imaging and monitoring of the PS activation. Upon image-guided light illumination, the green fluorescence of TPS residue is generated by apoptosis induced caspase-3/-7 activation, which is used for monitoring of the cell apoptosis and evaluation of the therapeutic responses. As compared with the

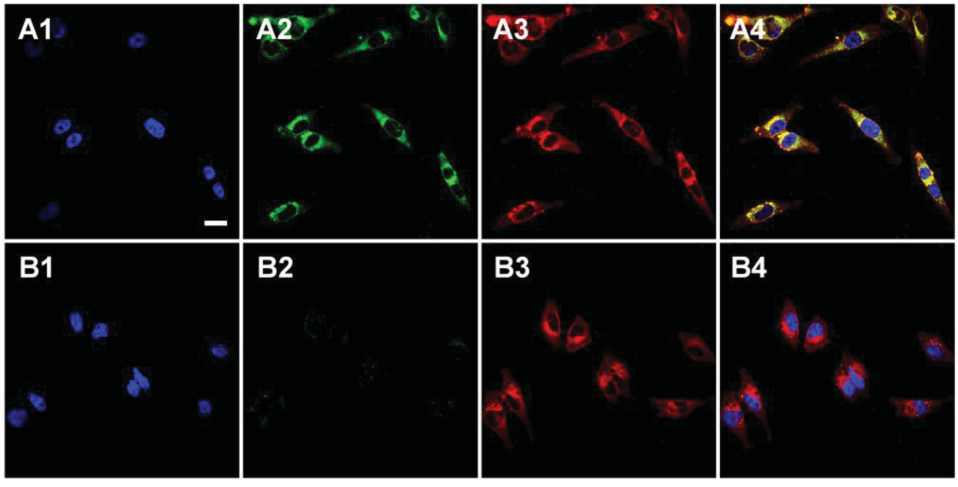

Figure 9. Confocal images of MDA-MB-231 cells upon treatment with the probe (10×10^{-6} M) in the absence (A1–A4) and in the presence (B1–B4) of caspase-3/-7 inhibitor with light irradiation. The blue fluorescence is from the nuclei of cells stained by Hoechst, the green fluorescence is from the TPS residue (E_x: 405 nm; E_m: 505–525 nm), the red fluorescence is from Texas Red-labeled secondary antibody (E_x: 543 nm; E_m: 610–640). A4 and B4 are the overlay images of (A1, A2, A3) and (B1, B2, B3), respectively. The scale bar is 20 μm.

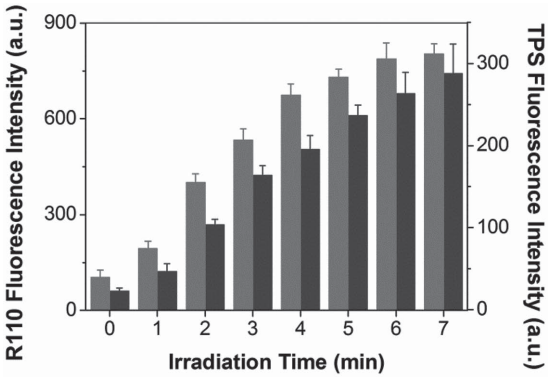

Figure 10. Cytotoxicity fluorescence intensity monitored using CytoTox-Fluor cytotoxicity assay and the intrinsic TPS residue fluorescence intensity change of MDA-MB-231 cells upon treatment with the probe (10×10^{-6} M) for 4 h with different durations of light irradiation.

previously reported molecular probes that can only monitor a single process of drug activation or therapeutic response, simultaneous monitoring of the whole processes is able to provide a clearer picture for further improved cancer therapy. We anticipate that the integrated probe design will offer new opportunities for cancer therapy and early evaluation of the therapeutic response will help to forecast specific therapeutic regimes for individual patient to help realize the ultimate goal of personalized medicine. Based on the proof-of-concept probe design in this work, further development of new AIEgens through molecular design with longer absorption and emission wavelengths for direct in vivo application is our next goal.

Supporting Information

Supporting Information is available from the Wiley Online Library or from the author.

Acknowledgements

Y.Y. and C.-J.Z. contributed equally to this work. The authors gratefully acknowledge the financial support from SMART (R279–000–378–592), the Ministry of Education (R279–000–391–112), Singapore NRF Investigatorship (R-279–000–444–281, R-279–000–444–282), and the Institute of Materials Research and Engineering of Singapore (IMRE/14–8P1110).

Received: July 4, 2015
Revised: August 23, 2015
Published online: October 8, 2015

[1] J. M. Gallo, P. Vicini, A. Orlansky, S. L. Li, F. Zhou, J. G. Ma, S. Puffer, M. A. Bookman, P. Guo, *Clin. Cancer Res.* **2004**, *10*, 8048.
[2] R. Langer, *Nature* **1998**, *392*, 5.
[3] S. L. Luo, E. L. Zhang, Y. P. Su, T. M. Cheng, C. M. Shi, *Biomaterials* **2011**, *32*, 7127.
[4] P. Zrazhevskiy, M. Sena, X. H. Gao, *Chem. Soc. Rev.* **2010**, *39*, 4326.
[5] M. H. Lee, Z. Yang, C. W. Lim, Y. H. Lee, S. Dongbang, C. Kang, J. S. Kim, *Chem. Rev.* **2013**, *113*, 5071.
[6] S. Bhuniya, S. Maiti, E. J. Kim, H. Lee, J. L. Sessler, K. S. Hong, J. S. Kim, *Angew. Chem. Int. Ed.* **2014**, *53*, 4469.
[7] T. T. Zou, C. T. Lum, S. S. Y. Chui, C. M. Che, *Angew. Chem. Int. Ed.* **2013**, *52*, 2930.
[8] Y. Y. Yuan, Y. L. Chen, B. Z. Tang, B. Liu, *Chem. Commun.* **2014**, *50*, 3868.
[9] J. N. Liu, J. W. Bu, W. B. Bu, S. J. Zhang, L. M. Pan, W. P. Fan, F. Chen, L. P. Zhou, W. J. Peng, K. L. Zhao, J. L. Du, J. L. Shi, *Angew. Chem. Int. Ed.* **2014**, *53*, 4551.
[10] X. L. Hu, G. H. Liu, Y. Li, X. R. Wang, S. Y. Liu, *J. Am. Chem. Soc.* **2015**, *137*, 362.
[11] X. D. Xue, Y. Y. Zhao, L. R. Dai, X. Zhang, X. H. Hao, C. Q. Zhang, S. D. Huo, J. Liu, C. Liu, A. Kumar, W. Q. Chen, G. Z. Zou, X. J. Liang, *Adv. Mater.* **2014**, *26*, 712.
[12] Y. Z. Min, J. M. Li, F. Liu, E. K. L. Yeow, B. G. Xing, *Angew. Chem. Int. Ed.* **2014**, *53*, 1012.
[13] R. Kumar, J. Han, H. J. Lim, W. X. Ren, J. Y. Lim, J. H. Kim, J. S. Kim, *J. Am. Chem. Soc.* **2014**, *136*, 17836.
[14] D. E. Dolmans, D. Fukumura, R. K. Jain, *Nat. Rev. Cancer* **2003**, *3*, 380.
[15] L. Cheng, C. Wang, L. Z. Feng, K. Yang, Z. Liu, *Chem. Rev.* **2014**, *114*, 10869.
[16] A. Gomes, E. Fernandes, J. L. F. C. Lima, *J. Biochem. Biophys. Methods* **2005**, *65*, 45.
[17] K. Y. Pu, A. J. Shuhendler, J. H. Rao, *Angew. Chem. Int. Ed.* **2013**, *52*, 10325.
[18] S. Kim, T. Tachikawa, M. Fujitsuka, T. Majima, *J. Am. Chem. Soc.* **2014**, *136*, 11707.
[19] P. R. Ogilby, *Chem. Soc. Rev.* **2010**, *39*, 3181.
[20] J. W. Tian, L. Ding, H. X. Ju, Y. C. Yang, X. L. Li, Z. Shen, Z. Zhu, J. S. Yu, C. J. Yang, *Angew. Chem. Int. Ed.* **2014**, *53*, 9544.
[21] G. Zheng, J. Chen, K. Stefflova, M. Jarvi, H. Li, B. C. Wilson, *Proc. Natl. Acad. Sci. USA* **2007**, *104*, 8989.
[22] J. F. Lovell, T. W. B. Liu, J. Chen, G. Zheng, *Chem. Rev.* **2010**, *110*, 2839.
[23] Q. Yuan, Y. Wu, J. Wang, D. Q. Lu, Z. L. Zhao, T. Liu, X. B. Zhang, W. H. Tan, *Angew. Chem. Int. Ed.* **2013**, *52*, 13965.
[24] J. W. Tian, L. Ding, H. J. Xu, Z. Shen, H. X. Ju, L. Jia, L. Bao, J. S. Yu, *J. Am. Chem. Soc.* **2013**, *135*, 18850.
[25] Y. Ichikawa, M. Kamiya, F. Obata, M. Miura, T. Terai, T. Komatsu, T. Ueno, K. Hanaoka, T. Nagano, Y. Urano, *Angew. Chem. Int. Ed.* **2014**, *53*, 6772.
[26] Y. Yuan, C. Zhang, B. Liu, *Angew. Chem. Int. Ed.* **2015**, DOI: 10.1002/anie.201503640.
[27] R. T. Kwok, C. W. Leung, J. W. Lam, B. Z. Tang, *Chem. Soc. Rev.* **2015**, *44*, 4228.
[28] D. Ding, K. Li, B. Liu, B. Z. Tang, *Acc. Chem. Res.* **2013**, *46*, 2441.
[29] X. Zhang, X. Zhang, L. Tao, Z. Chi, J. Xu, Y. Wei, *J. Mater. Chem. B* **2014**, *2*, 4398.
[30] X. R. Wang, J. M. Hu, G. Y. Zhang, S. Y. Liu, *J. Am. Chem. Soc.* **2014**, *136*, 9890.
[31] A. Shao, Y. Xie, S. Zhu, Z. Guo, J. Guo, P. Shi, T. D. James, H. Tian, W. H. Zhu, *Angew. Chem. Int. Ed.* **2015**. *54*, 7275.
[32] W. Qin, K. Li, G. X. Feng, M. Li, Z. Y. Yang, B. Liu, B. Z. Tang, *Adv. Funct. Mater.* **2014**, *24*, 635.
[33] Y. T. Gao, G. X. Feng, T. Jiang, C. C. Goh, L. G. Ng, B. Liu, B. Li, L. Yang, J. L. Hua, H. Tian, *Adv. Funct. Mater.* **2015**, *25*, 2857.
[34] E. P. J. Parrott, N. Y. Tan, R. R. Hu, J. A. Zeitler, B. Z. Tang, E. Pickwell-MacPherson, *Mater. Horizons* **2014**, *1*, 251.
[35] F. Hu, Y. Y. Huang, G. X. Zhang, R. Zhao, H. Yang, D. Q. Zhang, *Anal. Chem.* **2014**, *86*, 7987.
[36] Y. Yuan, C. J. Zhang, M. Gao, R. Zhang, B. Z. Tang, B. Liu, *Angew. Chem. Int. Ed.* **2015**, *54*, 1780.
[37] Q. L. Hu, M. Gao, G. X. Feng, B. Liu, *Angew. Chem. Int. Ed.* **2014**, *53*, 14225.

[38] A. C. Wood, P. Elvin, J. A. Hickman, *Br. J. Cancer* **1995**, *71*, 937.
[39] H. U. Simon, A. Haj-Yehia, F. Levi-Schaffer, *Apoptosis* **2000**, *5*, 415.
[40] M. Higuchi, T. Honda, R. J. Proske, E. T. H. Yeh, *Oncogene* **1998**, *17*, 2753.
[41] S. J. Riedl, Y. G. Shi, *Nat. Rev. Mol. Cell Biol.* **2004**, *5*, 897.
[42] J. Mei, Y. N. Hong, J. W. Y. Lam, A. J. Qin, Y. H. Tang, B. Z. Tang, *Adv. Mater.* **2014**, *26*, 5429.
[43] C. S. Foote, *Photochem. Photobiol.* **1991**, *54*, 659.
[44] S. Y. Lee, T. Yasuda, Y. S. Yang, Q. S. Zhang, C. Adachi, *Angew. Chem. Int. Ed.* **2014**, *53*, 6402.
[45] H. Shi, J. Liu, J. Geng, B. Z. Tang, B. Liu, *J. Am. Chem. Soc.* **2012**, *134*, 9569.
[46] A. Kamkaew, S. H. Lim, H. B. Lee, L. V. Kiew, L. Y. Chung, K. Burgess, *Chem. Soc. Rev.* **2013**, *42*, 77.
[47] A. Degterev, M. Boyce, J. Yuan, *Oncogene* **2003**, *22*, 8543.
[48] A. Luhrmann, C. V. Nogueira, K. L. Carey, C. R. Roy, *Proc. Natl. Acad. Sci. USA* **2010**, *107*, 18997.
[49] Y. S. Zhao, R. Bachelier, I. Treilleux, P. Pujuguet, O. Peyruchaud, R. Baron, P. Clement-Lacroix, P. Clezardin, *Cancer Res.* **2007**, *67*, 5821.
[50] M. Hultberg, B. Hultberg, *Chem. Biol. Interact.* **2006**, *163*, 192.